

Hyperspectral object classification using hybrid spectral-spatial fusion and noise tolerant soft-margin technique

Radhakrishna Mani, Manjunatha Raguttapalli Chowdareddy

Department of Electronics and Communication Engineering, Global Academy of Technology, Affiliated to Visvesvaraya Technological University, Bengaluru, India

Article Info

Article history:

Received Oct 10, 2023

Revised Nov 25, 2023

Accepted Dec 13, 2023

Keywords:

Class imbalance

Deep learning

Hybrid fusion

Hyperspectral imaging

Machine learning

Object classification

ABSTRACT

Because of its spectral-spatial and temporal resolution of greater areas, hyperspectral imaging (HSI) has found widespread application in the field of object classification. The HSI is typically used to accurately determine an object's physical characteristics as well as to locate related objects with appropriate spectral fingerprints. As a result, the HSI has been extensively applied to object identification in several fields, including surveillance, agricultural monitoring, environmental research, and precision agriculture. However, because of their enormous size, objects require a lot of time to classify; for this reason, both spectral and spatial feature fusion have been completed. The existing classification strategy leads to increased misclassification, and the feature fusion method is unable to preserve semantic object inherent features; This study addresses the research difficulties by introducing a hybrid spectral-spatial fusion (HSSF) technique to minimize feature size while maintaining object intrinsic qualities; Lastly, a soft-margins kernel is proposed for multi-layer deep support vector machine (MLDSVM) to reduce misclassification. The standard Indian pines dataset is used for the experiment, and the outcome demonstrates that the HSSF-MLDSVM model performs substantially better in terms of accuracy and Kappa coefficient.

This is an open access article under the [CC BY-SA](https://creativecommons.org/licenses/by-sa/4.0/) license.



Corresponding Author:

Radhakrishna Mani

Department of Electronics and Communication Engineering, Global Academy of Technology, Affiliated to Visvesvaraya Technological University

Bengaluru, Karnataka, India

Email: rk123research@gmail.com

1. INTRODUCTION

Remote-sensing images are those that are obtained using remote-sensing sensors, such as those supplied by satellites and drones. The main source of worldwide coverage, offering photographs of every region on Earth, is satellite imagery. In this approach, satellite imaging is used in many sectors, such as forestry, agriculture, oceanography, weather studies, and shoreline studies. It works especially effectively in the domains of precision agriculture and plant phenotyping identification [1], [2]. One such indicator is the normalized-difference vegetation index (NDVI) [3], from which the NDVI distributed mapping is typically derived using standard methods, which typically use the initial unmanned aerial vehicle (UAV) multi-spectral (MS) image. Inaccuracy in the NDVI distributed mapping could be caused by the original MS pictures' low spatial resolution. When compared to spectral resolution, MS picture spatial resolution is typically inadequate. Hyperspectral images (HSI) and panchromatic (Pan) images have low spectral resolution and high spatial resolution, respectively [4]. Utilizing MS images results in the loss of certain spatial information. Consequently, it is possible to simultaneously improve the spectral and spatial resolutions of the combined

MS and HSI. This trend encouraged the proposed research to design an effective hybrid fusion, i.e., spatial-spectral fusion technique for object classification. The resultant NDVI distributed mapping will have higher resolution and improve object classification performance.

One of the primary requirements that must be fulfilled before the satellite images can be utilized for object categorization applications is high resolution. Hyperspectral sensors produce images with high spectral information but low spatial information. However, multispectral sensors are image sensors that capture both a large amount of geographical data and a small amount of spectral information. A preprocessing technique called image-fusion enhances an image's spectral and spatial resolution. As illustrated in Figure 1, the image fusion method finds application in many domains, including medical image visualization, machine vision [5], bioinformatics security, land classification, navigation, variation identification, digital imaging, military applications, satellite, and aerial imaging [6], [7], robotic vision, food microbe detection [8], photography, and surveillance [9]. The goal of this study is to examine current advancements in image-fusion techniques used in HSI-based object classification methods, pinpoint issues and difficulties encountered, and provide a successful feature-fusion method that preserves intrinsic object characteristics in both spatial and spectral domains.

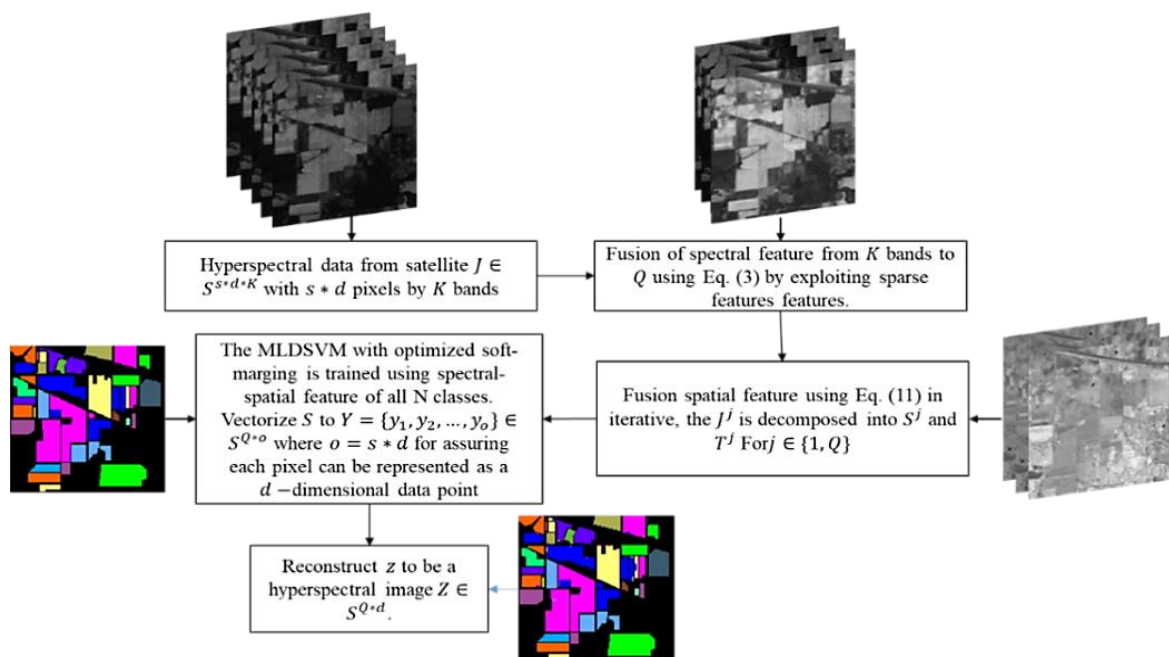


Figure 1. Architecture of proposed hybrid HSI fusion technique for object classification

The image-fusion approach [10] considers two photographs from the same area taken by different sensors; the main goal is to enhance the spatial and spectral resolution of one image without compromising the quality of the information about the intrinsic characteristics of the object. The present techniques aid in creating a fusion image with a better resolution, but there is a chance that the unwanted artifacts and noise elements caused by inadequate registration will affect how the fused image looks overall in the source photos. The enhanced quality of the final fused image will appear significantly different, depending on the task at hand and the source image. The most crucial stage in understanding the significance of the fusion process is evaluating the image quality. The objectives of object categorization applications [11] vary, thus choosing the best image fusion technique is essential. It can be challenging to choose the best method for implementing remote sensing object classification, especially in supervised classification environments where the "Hughes-phenomenon" exists because of an imbalance between the small training sample size and the extremely high spectral dimensions of HSI, which have negative effect on classification accuracy [11], [12]. This work presents a hybrid fusion technique namely hybrid spatial-spectral fusion (HSSF), where feature fusion is carried out both spatially and spectrally. Ultimately, a multi-layer deep support vector machine (MLDSVM) method is employed to accomplish object classification utilizing the spatial-spectral fused feature. The significance of the research work is given as:

- The article presents a spectral feature fusion process that minimizes the total number of bands needed for hyperspectral imaging-based item categorization.
- Second, a spatial feature fusion process that preserves and minimizes each object's intrinsic properties was introduced by the work.
- Lastly, a new soft-margin weights optimization for a multi-layer deep support vector machine classification algorithm was presented that lowers misclassification.

The paper's organization is as follows: section 2 examines the limitations of the many image fusion and classification methods currently in use for the application of remote sensing object categorization. The hybrid fusion technique's suggested methodology is presented in section 3. The experiment investigation and comparison with the current fusion-based object categorization methodology are presented in section 4. Finally, a direction for further research was suggested in the research conclusion.

2. LITERATURE SURVEY

This section studies various existing fusion and classification techniques for improving the quality of satellite images for effective provisioning of remote sensing object classification applications. In study [13] showed outlier [14] during the registration process significantly impacts fusion performance; recently, deep learning-based techniques [15] have been used to effectively remove the outliers and enhance fusion accuracy [16]. Using spatial data from HSI characteristics, an HSI-based crop classification model was developed in [17]. Lastly, crop categorization is carried out to estimate large-scale crop areas. They analyzed precision in the early-seasonal predicting approach and modeled a transfer learning approach using growing season data. For improved crop-type mapping, multispectral time-series data and synthetic-aperture radar data were integrated in [18]. They demonstrated how inaccurate it is to only use radar data, determined which feature combination improves accuracy, and researched misclassification to improve crop profile modeling. They looked at two different fusion techniques and demonstrated how feature selection helps cut down on computational overhead. Yin *et al.* [19] explored fusion methods for scene classification using HSI, taking into account several points of view. They assessed scene classification with both single-side and multiple-side image combinations [20]. Recent convolution neural network (CNN)-based crop categorization techniques and their advantages for precise outcomes were examined in [21]. To achieve better fusion, Zhang *et al.* [22] presented a CNN that combines interleaving perception; the model is concentrated on fusing heterogeneous information from light detection and ranging (LiDAR) data and HSI. A bidirectional autoencoder was created to perform the reconstruction of LiDAR and HSI features together. The fused information is then fed into a two-branch CNN to perform classification. Gao *et al.* [23] created a technique for identifying the land cover of complicated wetlands with patchy, mixed vegetation. First, CNN is utilized to merge the HSI and multispectral characteristics. After the model ensures a high quality of spatial-spectral feature resolution, pixel-by-pixel object classification is carried out using the fused image's spatial and spectral visual correlation. The fusion method known as enhanced multiscale feature-fusion network (EMFFN) was first introduced in [24]. Using two subnetworks, the spectral cascaded dilated convolutional network (SCDCN) and parallel multipath network (PMN), the model extracts multiscale spatial-spectral information [25]. When extracting multiscale characteristics from long-range data of bigger fields, the SCDCN is employed. Next, small, medium, and large-scale features are spatially captured using PMN. In the end, a hierarchical fusion of features ensures improved high-level semantic features even with insufficient training data [26], [27]

3. PROPOSED METHOD

This section introduces an effective HSI fusion technique that reduces the band and feature size and retains high-quality features both spatially and as well as spectrally. Finally, using the fused features information the object classification process is done using a machine learning algorithm. The architecture of the proposed HSI object classification methods is given in Figure 1.

3.1. Spectral-spatial feature fusion technique

The raw HSI J with band size of K can be expressed using (1).

$$J = (J_1, \dots, J_O) \in \mathcal{S}^{C \times O} \quad (1)$$

where K is represented as $\mathcal{S}^{C \times O}$, the raw HSI is segmented into N clusters with equal spectral band size, the parameter C defines dimensions and parameter O defines the pixel size of raw HSI. The band size in each cluster is expressed as (2).

$$C_1, C_2, \dots, C_N \tag{2}$$

The averaging-based image fusion is done at each group and the corresponding fusion data Q is given using (3).

$$\tilde{J}_n = \frac{\sum_{o=1}^{C_n} J_n^o}{C_n} \tag{3}$$

where parameter n defines the n^{th} group, C_n defines the band's size in the n^{th} group, J_n^o defines the o^{th} band in the n^{th} group of the raw HSI, and \tilde{J}_n defines the n^{th} spectral band after performing fusion. In (3) enables the spectrally reduced pixels of HSI to retain the object's physical properties i.e., quality of object reflectance will be retained. Further, the model is very effective in eliminating noise. The spectrally reduced HSI \tilde{J} is again divided into multiple sub-clusters of neighboring bands as defined in (4).

$$\tilde{J}^l = \begin{cases} (\tilde{J}_{(l-1)A+1}, \dots, \tilde{J}_{(l-1)A+A}), l = 1, 2, \dots, \lfloor \frac{N}{A} \rfloor \\ (\tilde{J}_{N-A+1}, \dots, \tilde{J}_N), l = \lceil \frac{N}{A} \rceil \neq \lfloor \frac{N}{A} \rfloor \end{cases} \tag{4}$$

where \tilde{J}^l defines the l^{th} subcluster, A defines the band size of each cluster, $\lfloor \frac{N}{A} \rfloor$ represents the minimum value not smaller than $\frac{N}{A}$, $\lceil \frac{N}{A} \rceil$ represents the maximum value not larger than $\frac{N}{A}$. Then, for obtaining shading and reflectance features of each object optimization is done using an intrinsic feature extraction mechanism at each subcluster \tilde{J}^l as defined in (5).

$$(T^{l*}, S^{l*}) = \arg \min_{S^l, T^l} E(\tilde{J}^l, \hat{S}^l, \hat{T}^l) \tag{5}$$

where T^l defines shading elements of the l^{th} subcluster and S^l defines reflectance elements of the l^{th} subcluster. Finally, the reflectance features of objects in multiple subclusters are fused to obtain the corresponding intrinsic features of objects, which is defined as a matrix representation with n -dimensional feature \tilde{S} as defined in (6).

$$\tilde{S} = \begin{pmatrix} S^1 \\ \vdots \\ S^l \\ \vdots \\ S^{\lfloor \frac{N}{A} \rfloor} \end{pmatrix} \in \mathcal{S}^{N \times O} \tag{6}$$

The intrinsic feature depends on the surface feature of the earth; the illumination and climate conditions impact the intrinsic properties of objects. To extract semantically meaningful features spatially the shading feature must be removed from the intrinsic feature. Let the intensity feature, intrinsic feature, and shading feature be defined using parameters $J \in \mathcal{S}^{s \times d}$, $S \in \mathcal{S}^{s \times d}$, and $T \in \mathcal{S}^{s \times d}$, respectively. The HSI for a pixel q is expressed as a pixel-wise multiplicative of object reflectance and shading features as defined in (7).

$$J_q = S_q T_q \tag{7}$$

where q represents pixel indexes. In (7), the parameters S_q and T_q are unknown parameters and J_q is the known parameter. The reflectance properties of objects will vary extremely at the edges and remain similar within the respective object class. The value of reflectance keeps changing with variation in intensity value; thus, identifying the exact intensity value will result in identifying similar reflectance output. Therefore, reflectance S_q is measured as (8).

$$S_q = \sum_{r \in \mathcal{O}(q)} b_{qr} S_r \tag{8}$$

In (8), b_{qr} defines the parameter that estimates intensity similarities between spectral angle and intensity value among pixel indexes q and r . In measuring b_{qr} affinity graph through the Gaussian function both the range distance between intensity J_q and J_r and the space distance between pixel q and r are used through (9),

$$b_{qr} = \begin{cases} \exp \left[- \left(\frac{\|q-r\|_2^2}{2\sigma_t^2} + \frac{\|J_q - J_r\|_2^2}{2\sigma_s^2} \right) \right], & \text{if } r \in \mathcal{O}(q) \\ 0, & \text{otherwise} \end{cases} \quad (9)$$

where σ_t defines the space optimization parameter and σ_s defines the range optimization parameter. Therefore, using (9), the S_r can be established through (10).

$$S_r = \sum_{r \in \mathcal{O}(q)} \left\{ \exp \left[- \left(\frac{\|q-r\|_2^2}{2\sigma_t^2} + \frac{\|J_q - J_r\|_2^2}{2\sigma_s^2} \right) \right] \right\} S_r \quad (10)$$

Using (9) the HSI J_q structure can be preserved with better texture S_q representation. The object intrinsic feature is established by considering $\tilde{T}_q = \frac{1}{J_q}$ through linear properties using (7) and (8).

$$\begin{cases} S_q = \sum_{r \in \mathcal{O}(q)} b_{qr} S_r, \\ \tilde{T}_q = \frac{1}{J_q} S_r, \end{cases} \quad (11)$$

Using (11), the value of S_q and T_q is approximated to decompose J^j to S^j and $T^j \forall j \in \{1, Q\}$. Therefore, the reflectance value of different objects by eliminating shading is obtained. Thus, aiding in better spatial feature intrinsic representation. Once the fusion of both spectral and spatial is done. The final fused feature of S of different objects is represented as a vector form defined as Y and trained using the machine learning algorithm defined below.

3.2. Multi-layer deep support vector machine model

The feature space of objects is expressed as $Y \in S^e$, the index is defined as $Z = \{-1 + 1\}$, and the corresponding object distribution considering $Y * Z$ is defined as E . The margin of standard SVM is computed as (12).

$$\beta_j = z_j x^U \alpha(y_j), \quad j = 1, 2, 3, \dots, n \quad (12)$$

where $\alpha(y_j)$ defines feature mapping of y to kernel L . The traditional SVM [28] is usually designed through the assumption that the object is distinguishable and hyperplane have the competence to classify the object feature T with minimal false positives; therefore, the SVM margin is estimated as (13).

$$\min_x \frac{1}{2} \|x\|^2 \text{ such that } z_j x^U \alpha(y_j) \geq 1, \quad j = 1, 2, 3, \dots, n, \quad (13)$$

However, when crops have comparable characteristics, when data is unbalanced, or when crops are classified in a mixed cropping setting, using the aforementioned in (13) will result in high misclassification. Moreover, there are situations in which certain crops have relatively few features available, while other crops have many features available; this can cause problems with data imbalance. The outcome of applying the SVM classification constructed with the hard margin given in the preceding equation is not that good. In light of data imbalance and the presence of label-noise concerns, this work introduces soft-margin with multi-layer deep SVM for optimizing the decision boundary for crop classification. By concurrently maximizing the margin average and lowering the margin difference, the proposed multi-layer deep SVM model optimizes the decision boundary and its difference is calculated using (12).

$$\hat{\beta} = \frac{1}{n^2} \sum_{j=1}^n \sum_{k=1}^n [z_j x^U \alpha(y_j) - z_k x^U \alpha(y_k)]^2 \quad (14)$$

and the margin average is computed through (15).

$$\bar{\beta} = \frac{1}{n} \sum_{j=1}^n z_j x^U \alpha(y_j) = \frac{1}{n} (YZ)^U x, \quad (15)$$

Using (16), the optimization of the decision boundary is updated as (16).

$$\min_x \frac{1}{2} \|x\|^2 + \delta_1 \hat{\beta} - \delta_2 \bar{\beta} \text{ such that } \alpha(y_j) \geq 1, \quad j = 1, 2, 3, \dots, n \quad (16)$$

where δ_1 and δ_2 are bounds utilized in getting optimal performance. The work further develops an effective margin maximization and error minimization to classify the object T which are indistinguishable using (17).

$$\min_{x, \mu} \frac{1}{2} \|x\|^2 \delta_1 \hat{\beta} - \delta_2 \bar{\beta} + D \sum_{j=1}^n \mu_j \text{ such that } z_j x^U \alpha(y_j) \geq 1 - \mu_j, \mu_j \geq 0, j = 1, 2, 3, \dots, n, \quad (17)$$

where variable D is a regularization term used for optimizing penalty for wrong classification, and in measuring feature loss the work uses slack variable μ ; in this work higher penalty is given for larger error.

The classifier construction for multi-label object classification using MLDSVM is done using a pairwise-based mechanism. Let's consider there is Z number of object classes where $Z = \{1, 2, \dots, m\}$, and $m(m-1/2)$ hyperplane is constructed on all probabilistic pairwise classifiers employing MLDSVM. The MLDSVM initially carryout binary classification between two classes j and k using function $f_{jk}(y) \in \{-1, 1\}$ where $j \neq k \in Z$. In this work, before making any prediction y_q , it is essential to compute the weighted function $T_j(y_q)$ of each class $j \in Z$ to differentiate between the classes as defined through (18).

$$T_j(y_q) = \sum_{\substack{k=1 \\ k \neq j}}^m \text{sgn}\{g_{jk}(y_q)\} \quad (18)$$

where $\text{sgn}(\cdot)$ defines signum function which is used for getting the real value of binary classification. The classification outcome y_q is obtained according to maximum weighted objects as expressed through (19).

$$j^* = \arg \max_{j \in Z} \{T_j(y_q)\}. \quad (19)$$

The adoption of hybrid spatial-spectral fusion combined with MLDSVM aids in attaining higher accuracy in comparison with a traditional model which is experimentally shown in the next section.

4. RESULT AND DISCUSSION

In this section, the performance of the HSSF-MLDSVM based hyper-spectral image object classification using HSI has been compared with the other existing feature fusion-based object classification techniques spectral-spatial dependent global learning (SSDGL) [10], central attention network (CAN) [11], convolution neural network -active learning-Markov random field (CNN-AI-MNF) [12], enhanced-multiscale feature-fusion network (EMFFN) [24], 3-dimension self-attention multiscale feature-fusion network (3DSA-MFN) [25], adaptive spectral-spatial feature fusion network (ASSFFN) [26], low-rank attention multiple feature-fusion network (LMAFN) [27], and deep support vector machine (DSVM) [28]. For evaluating the proposed HSSF-MLDSVM and other existing HSI object classification techniques, the Indian Pines dataset has been used. Overall-accuracy (OA), average-accuracy (AA), the kappa-coefficient (K), and time required for computation are some of the most commonly utilized metrics in current HSI-based object classification techniques to evaluate the effectiveness of various HSI fusion based object-classification approaches. By attaining higher values for the OA, AA, and K, the technique shows the best performance. Moreover, by decreasing the time for the computation, the techniques can be deployed in real-time.

4.1. Dataset description

An airborne visible-infrared imaging spectrometer (AVIRIS) sensor that was positioned over the northwestern corner of Indiana was used for capturing the data for the Indian-Pines dataset as shown in Figure 2. When gathering hyperspectral information, a wavelength of $0.4\text{-}2.5 \times 10^{-6}$ meters is used alongside 145×145 pixels and 224 bands. Indian-Pines Dataset is necessary since two-thirds of the area that was measured is agricultural, while the remaining one-third is made up of forest along with other naturally present flora. Indian-Pines dataset also includes two-lane highways, two-way streets, residential neighborhoods, and other low-rise structures. In addition, some crops are still in the beginning phases of their development, which accounts for fewer than five percent of the total data acquired in the Indian Pines dataset. According to Figure 2, there are an overall 16 crops (or labels) that make up the ground-truth information. In a manner comparable to [10], and [11], the water-absorption spectrum bands are removed, and the total number of the bands that comprise the spectral spectrum is decreased to 200.

4.2. Study the classification performance of the proposed method used for object classification

In this section the significance of proposed classifier employing HSSF and its classification accuracy and Kappa coefficient graphical outcome have been studied in Figure 3. The results show the proposed model without HSSF achieved an average accuracy of 81.45% and Kappa coefficient of 82.61% for

Indian-pines HSI. On the other side, the proposed model with HSSF achieves an average accuracy of 99.93% and Kappa coefficient of 99.91%. Thus, results show employing HSSF aids in significantly improving classification accuracy by reducing misclassification.

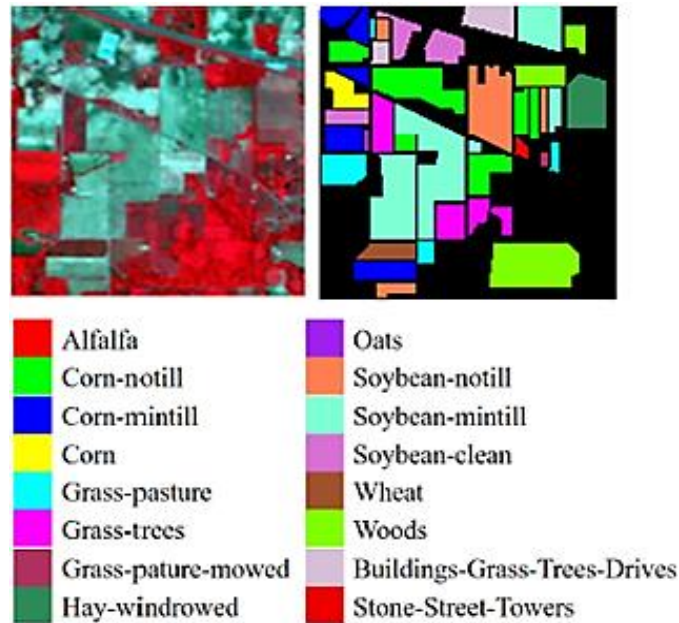


Figure 2. Pseudo-color image and ground-truth map for Indian Pines dataset

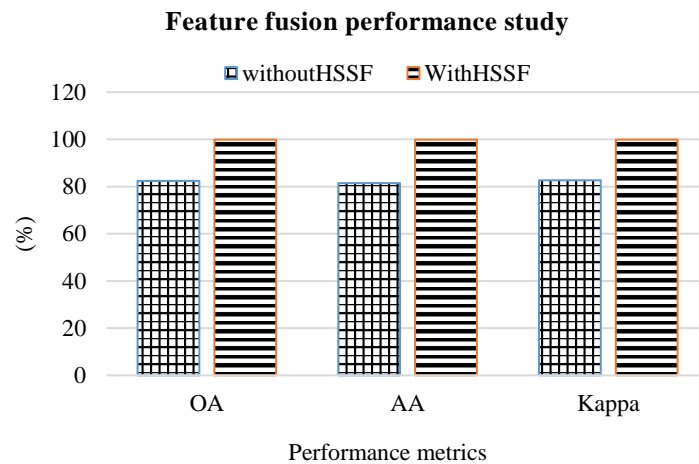


Figure 3. Spatial-spectral performance study on object classification

4.3. Comparative study

In this section, the experimentation has been done using the Indian-pines dataset and has been evaluated using the OA, AA, K, and time required for the computation metrics. The proposed HSSF-SVM technique has been compared with the existing techniques like SSDGL, CAN, CNN-AI-MNF, EMFFN, 3DSA-MFN, ASSFFN, LMAFN, and DSVM techniques. The accuracy that has been achieved for the various objects (class name) has been given in Table 1. From the results presented in Table 1, it can be noted that the presented HSSF-SVM technique attains the best accuracy in terms of OA, AA, K, and time required for the computation for all the objects in comparison to the other existing techniques. Moreover, the proposed HSSF-SVM technique induces the least computing overhead when compared with all the CNN-AL-MNF and EMFFN techniques.

4.4. Classification map comparison

Figure 4 shows the classification produced by existing HSI object classification methods. The accuracies of different existing HSI object classification methods are given inside the parenthesis. The result clearly shows the proposed method produces very high accuracies by reducing the false positive in comparison with existing HSI object classification methods; thus, produces better classification maps in comparison with existing HSI object classification methods.

Table 1. Comparative analysis

Class name	DSVM (2020) [28]	CNN-AI-MNF (2020) [12]	SSDGL (2022) [10]	CAN (2021) [11]	EMFFN (2021) [24]	3DSA-MFN (2022) [25]	ASSFFN (2022) [26]	LMAFN (2023) [27]	HSSF- MLDSVM [Proposed]
Alfalfa	100	92.71	100	87.8	100	98.67	93.18	98.78	99.97
Corn notill	100	92.98	99.63	98.05	96.88	99.59	96.24	64.40	100
Corn mintill	100	88.7	99.24	97.99	99.22	100.00	97.85	66.02	100
Corn	100	97.7	100	94.37	99.97	98.73	97.35	90.95	100
Grass pasture	99.43	92.9	99.56	98.39	99.37	100.00	98.91	83.37	99.93
Grass trees	98.89	98.89	100	99.7	99.80	99.54	99.71	96.72	99.89
Grass pasture moved	100	76.74	100	100	100	100.00	40.74	99.57	100
Hay windrowed	98.72	97.87	100	100	100	99.09	100	99.70	99.98
Oats	100	38.89	100	77.78	100	99.42	84.21	100.00	99.97
Soybean notill	95.75	92.27	99.68	98.17	98.07	99.56	96.86	74.01	99.56
Soybean mintill	100	95.07	99.36	98.33	97.91	100.00	98.67	67.36	99.79
Soybean clean	99.63	90.51	99.11	97.94	99.31	99.56	96.98	80.43	100
Wheat	100	96.53	100	100	100	98.47	98.46	98.55	99.88
Woods	100	99.28	100	98.77	99.53	98.73	100	93.01	100
Buildings	95.45	88.4	100	92.51	99.55	99.37	100	86.90	99.87
grass trees									
Stone steel towers	100	97.12	100	98.81	99.73	99.37	98.88	98.30	100
OA (%)	98.86	98.79	99.63	98.1	98.85	99.52	98.11	75.41	99.91
AA (%)	99.24	94.28	99.79	96.16	-	99.32	93.62	78.15	99.93
Kappa (%)	-	-	99.58	97.84	98.36	99.24	97.84	87.38	99.91
Time (s)	-	8109.34	-	-	279.65	-	-	-	104.45

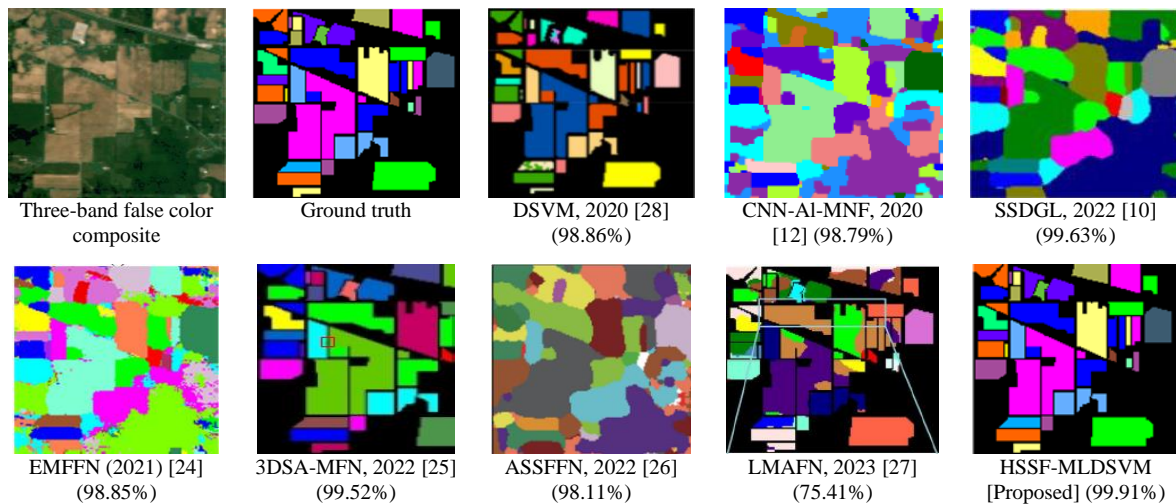


Figure 4. Classification maps produced using different HSI object classification methods

5. CONCLUSION

This paper discusses various current HSI classification method using different fusion method adopting machine learning, deep leaning, and hybrid feature fusion mechanism; however, the current method exhibit poor performance for classes with less features; thus, shows they are not effective handling class imbalance issues; further, research shows current method failed to handle the impact of noisy i.e., mixed-pixel; thus, failed to provide classification performance requirements of realistic platform; in this work a novel hybrid fusion method is developed combing feature of both spatial and spectral in more semantic manner; then, the fused feature of different object are trained with novel multi-layer deep SVM model to

perform object classification; experiment are conducted on two benchmark datasets; the result shows proposed method can handle both class imbalance and noisy mixed pixel problem using limited amount of training sample; the proposed HSSF-MLDSVM attains much improved performance in comparison with current HSI classification methodologies in terms of accuracy and Kappa coefficient. Future work would consider validating the model by introducing artificial noise representing more realistic HSI object classification scenarios.




REFERENCES

- [1] S. M. Panchal and Shivaputra, "Precise identification of objects in a hyperspectral image by characterizing the distribution of pure signatures," *International Journal of Electrical and Computer Engineering (IJECE)*, vol. 12, no. 6, pp. 6068–6078, Dec. 2022, doi: 10.11591/ijece.v12i6.pp6068-6078.
- [2] M. C. G. Babu and M. C. Padma, "Semantic feature extraction method for hyperspectral crop classification," *Indonesian Journal of Electrical Engineering and Computer Science (IJECS)*, vol. 23, no. 1, pp. 387–395, Jul. 2021, doi: 10.11591/ijeecs.v23.i1.pp387-395.
- [3] V. G. Vani and K. Thippeswamy, "Spatial-spectral feature for extraction technique for hyperspectral crop classification," *Indian Journal of Science and Technology*, vol. 15, no. 2, pp. 81–90, Jan. 2022, doi: 10.17485/IJST/v15i2.1810.
- [4] K. Zhang *et al.*, "Panchromatic and multispectral image fusion for remote sensing and earth observation: Concepts, taxonomy, literature review, evaluation methodologies and challenges ahead," *Information Fusion*, vol. 93, pp. 227–242, May 2023, doi: 10.1016/j.inffus.2022.12.026.
- [5] M. C. G. Babu and M. C. Padma, "Inherent feature extraction and soft margin decision boundary optimization technique for hyperspectral crop classification," *International Journal of Advanced Computer Science and Applications*, vol. 12, no. 12, pp. 684–692, 2021, doi: 10.14569/IJACSA.2021.0121285.
- [6] A. Asokan, J. Anitha, B. Patrut, D. Danculescu, and D. J. Hemanth, "Deep feature extraction and feature fusion for bi-temporal satellite image classification," *Computers, Materials and Continua*, vol. 66, no. 1, pp. 373–388, 2021, doi: 10.32604/cmc.2020.012364.
- [7] O. Tamin, E. G. Moung, J. A. Dargham, F. Yahya, and S. Omatu, "A review of hyperspectral imaging-based plastic waste detection state-of-the-arts," *International Journal of Electrical and Computer Engineering (IJECE)*, vol. 13, no. 3, pp. 3407–3419, Jun. 2023, doi: 10.11591/ijece.v13i3.pp3407-3419.
- [8] C. H. Feng, Y. Makino, S. Oshita, and J. F. G. Martín, "Hyperspectral imaging and multispectral imaging as the novel techniques for detecting defects in art and processed meat products: current state-of-the-art research advances," *Food Control*, vol. 84, pp. 165–176, Feb. 2018, doi: 10.1016/j.foodcont.2017.07.013.
- [9] S. Li, R. Dian, L. Fang, and J. M. Bioucas-Dias, "Fusing hyperspectral and multispectral images via coupled sparse tensor factorization," *IEEE Transactions on Image Processing*, vol. 27, no. 8, pp. 4118–4130, Aug. 2018, doi: 10.1109/TIP.2018.2836307.
- [10] Q. Zhu *et al.*, "A spectral-spatial-dependent global learning framework for insufficient and imbalanced hyperspectral image classification," *IEEE Transactions on Cybernetics*, vol. 52, no. 11, pp. 11709–11723, Nov. 2022, doi: 10.1109/TCYB.2021.3070577.
- [11] Z. Zhao, D. Hu, H. Wang, and X. Yu, "Center attention network for hyperspectral image classification," *IEEE Journal of Selected Topics in Applied Earth Observations and Remote Sensing*, vol. 14, pp. 3415–3425, 2021, doi: 10.1109/JSTARS.2021.3065706.
- [12] X. Cao, J. Yao, Z. Xu, and D. Meng, "Hyperspectral image classification with convolutional neural network and active learning," *IEEE Transactions on Geoscience and Remote Sensing*, vol. 58, no. 7, pp. 4604–4616, Jul. 2020, doi: 10.1109/TGRS.2020.2964627.
- [13] T. Kim, Y. Yun, C. Lee, J. Yeom, and Y. Han, "Image registration of very-high-resolution satellite images using deep learning model for outlier elimination," in *International Geoscience and Remote Sensing Symposium (IGARSS)*, Jul. 2022, pp. 155–158, doi: 10.1109/IGARSS46834.2022.9884075.
- [14] R. Feng, H. Shen, J. Bai, and X. Li, "Advances and opportunities in remote sensing image geometric registration: a systematic review of state-of-the-art approaches and future research directions," *IEEE Geoscience and Remote Sensing Magazine*, vol. 9, no. 4, pp. 120–142, Dec. 2021, doi: 10.1109/MGRS.2021.3081763.
- [15] N. S. Anil and D. Chandrappa, "A novel and efficient automatic hyperspectral image registration technique," *Procedia Computer Science*, vol. 171, pp. 2779–2786, 2020, doi: 10.1016/j.procs.2020.04.302.
- [16] A. N. ShambuGowda and C. D. Nanjundaiah, "Dynamic gradient sparsity based image registration and fusion technique for satellite images," in *Lecture Notes in Electrical Engineering*, vol. 903, Springer Nature Singapore, 2022, pp. 399–409.
- [17] L. P. Pott, T. J. C. Amado, R. A. Schwalbert, G. M. Corassa, and I. A. Ciampitti, "Satellite-based data fusion crop type classification and mapping in Rio Grande do Sul, Brazil," *ISPRS Journal of Photogrammetry and Remote Sensing*, vol. 176, pp. 196–210, Jun. 2021, doi: 10.1016/j.isprsjprs.2021.04.015.
- [18] A. Orynbaikyzy, U. Gessner, B. Mack, and C. Conrad, "Crop type classification using fusion of sentinel-1 and sentinel-2 data: assessing the impact of feature selection, optical data availability, and parcel sizes on the accuracies," *Remote Sensing*, vol. 12, no. 17, Aug. 2020, doi: 10.3390/rs12172779.
- [19] L. Yin, P. Yang, K. Mao, and Q. Liu, "Remote sensing image scene classification based on fusion method," *Journal of Sensors*, vol. 2021, pp. 1–14, Jun. 2021, doi: 10.1155/2021/6659831.
- [20] Z. Huang and S. Xie, "Classification method for crop by fusion hyper spectral and LiDAR data," in *2022 14th International Conference on Measuring Technology and Mechatronics Automation (ICMTMA)*, Jan. 2022, pp. 1011–1014, doi: 10.1109/ICMTMA54903.2022.00205.
- [21] A. Bouguettaya, H. Zarzour, A. Kechida, and A. M. Taberkit, "Deep learning techniques to classify agricultural crops through UAV imagery: a review," *Neural Computing and Applications*, vol. 34, no. 12, pp. 9511–9536, Mar. 2022, doi: 10.1007/s00521-022-07104-9.
- [22] M. Zhang, W. Li, R. Tao, H. Li, and Q. Du, "Information fusion for classification of hyperspectral and LiDAR data using IP-CNN," *IEEE Transactions on Geoscience and Remote Sensing*, vol. 60, pp. 1–12, 2022, doi: 10.1109/TGRS.2021.3093334.
- [23] Y. Gao *et al.*, "Fusion classification of HSI and MSI using aspatial-spectral vision transformer for wetland biodiversity estimation," *Remote Sensing*, vol. 14, no. 4, Feb. 2022, doi: 10.3390/rs14040850.




- [24] J. Yang, C. Wu, B. Du, and L. Zhang, "Enhanced multiscale feature fusion network for HSI classification," *IEEE Transactions on Geoscience and Remote Sensing*, vol. 59, no. 12, pp. 10328–10347, Dec. 2021, doi: 10.1109/TGRS.2020.3046757.
- [25] Y. Qing, Q. Huang, L. Feng, Y. Qi, and W. Liu, "Multiscale feature fusion network incorporating 3D self-attention for hyperspectral image classification," *Remote Sensing*, vol. 14, no. 3, Feb. 2022, doi: 10.3390/rs14030742.
- [26] H. Gao, Z. Chen, and F. Xu, "Adaptive spectral-spatial feature fusion network for hyperspectral image classification using limited training samples," *International Journal of Applied Earth Observation and Geoinformation*, vol. 107, Mar. 2022, doi: 10.1016/j.jag.2022.102687.
- [27] F. Feng, Y. Zhang, J. Zhang, and B. Liu, "Low-rank constrained attention-enhanced multiple spatial-spectral feature fusion for small sample hyperspectral image classification," *Remote Sensing*, vol. 15, no. 2, Jan. 2023, doi: 10.3390/rs15020304.
- [28] O. Okwuashi and C. E. Ndehedehe, "Deep support vector machine for hyperspectral image classification," *Pattern Recognition*, vol. 103, Jul. 2020, doi: 10.1016/j.patcog.2020.107298.

BIOGRAPHIES OF AUTHORS



Radhakrishna Mani    is a research scholar, Department of Electronics and Communication Engineering, Visvesvaraya Technological University, Karnataka, India. He completed BE in VTU, Karnataka and M.Tech. from JNTU, Hyderabad. Area of interest artificial intelligence, deep learning, machine learning, data mining and image processing. He can be contacted at email: rk123research@gmail.com.



Manjunatha Raguttapalli Chowdareddy    is an associate professor at Global Academy of Technology in Electronics and Communication Engineering Department. He holds a Ph.D. from Jain University, with his extensive knowledge and experience, he actively contributes to the Department of Electronics and Communication Engineering, enriching the learning experience for students and making significant contributions to the field of electronics and communication engineering. He can be contacted at email: manjunathrc84@gmail.com.